Modeling the Impact of COVID-19 on Air Quality in Southern California: Implications for Future Control Policies

Zhe Jiang[1, 2†], Hongrong Shi[1*†], Bin Zhao[3*], Yu Gu[4], Yifang Zhu[5], Kazuyuki Miyazaki[6], Xin Lu[7], Yuqiang Zhang[8], Kevin W. Bowman[4,6], Takashi Sekiya[9], Kuo-Nan Liou[4]

[1] Key Laboratory of Middle Atmosphere and Global Environment Observation, Institute of Atmospheric Physics, Chinese Academy of Sciences, Beijing, China
[2] Carbon Neutrality Research Center, Institute of Atmospheric Physics, Chinese Academy of Sciences, Beijing, China
[3] Pacific Northwest National Laboratory, Richland, WA, USA
[4] Joint Institute for Regional Earth System Science and Engineering and Department of Atmospheric and Oceanic Sciences, University of California, Los Angeles, CA, USA
[5] Institute of Environment and Sustainability, University of California, Los Angeles, CA, USA
[6] Jet Propulsion Laboratory, California Institute of Technology, Pasadena, CA, USA
[7] Petrochina North China Gas Marketing Company, Beijing, China
[8] Nicholas School of the Environment, Duke University, Durham, NC, USA
[9] Japan Agency for Marine-Earth Science and Technology, Yokohama, Japan

Correspon*dence to*: Hongrong Shi (shihrong@mail.iap.ac.cn) and Bin Zhao (bin.zhao@pnnl.gov)

† Zhe Jiang and Hongrong Shi contributed equally to this paper.

Abstract. In response to the Coronavirus Disease 2019 (COVID-19), California issued statewide stay-at-home orders, bringing about abrupt and dramatic reductions in air pollutant emissions. This crisis offers us an unprecedented opportunity to evaluate the effectiveness of emission reductions on air quality. Here we use the Weather Research and Forecasting model with Chemistry (WRF-Chem) in combination with surface observations to study the impact of the COVID-19 lockdown measures on air quality in southern California. Based on activity level statistics and satellite observations, we estimate the sectoral emission changes during the lockdown. Due to the reduced emissions, the population-weighted concentrations of fine particulate matter ($PM_{2.5}$) decrease by 15% in southern California. The emission reductions contribute 68% of the $PM_{2.5}$ concentration decrease before and after the lockdown, while meteorology variations contribute the remaining 32%. Among all chemical compositions, the $PM_{2.5}$ concentration decreases due to emission reductions is dominated by nitrate and primary components. For O_3 concentrations, the emission reductions cause a decrease in rural areas but an increase in urban areas; the increase can be offset by a 70% emission reduction in anthropogenic volatile organic compounds (VOC). These findings suggest that a strengthened control on primary $PM_{2.5}$ emissions and a well-balanced control on nitrogen oxides and VOC emissions are needed to effectively and sustainably alleviate $PM_{2.5}$ and O_3 pollution in southern California.

1 Introduction

Anthropogenic emissions from various emission sources, including transportation, industrial, agricultural, residential, and commercial sectors, contribute to California's long-existing air pollution problems (e.g., Shirmohammadi et al., 2016; Hong et al., 2015; Warneke et al., 2013). The major pollutants include, but are not limited to, fine particulate matter ($PM_{2.5}$), nitrogen dioxide (NO_2), sulfur dioxide (SO_2) and ozone (O_3). Exposure to these pollutants has been correlated with an increased rate of morbidity and mortality (Wang et al., 2019). Mitigating the adverse effects of air pollution by reducing air pollutant emissions from major sectors has been and will continue to be a major public policy challenge. However, the effect of emission reductions from various sources on air quality improvement is subject to substantial uncertainties, because such effect cannot be directly measured and because the atmospheric chemistry processes are highly nonlinear and complicated (Zhao et al., 2019b; Zhao et al., 2015; Chen et al., 2013). The recent Coronavirus Disease 2019 (COVID-19) pandemic provides an unprecedented opportunity for a more robust understanding of the environmental impacts brought by the emission reductions.

More than 200 countries and territories around the world have reported a total of about 53 million confirmed cases of the coronavirus COVID-19 that originated from Wuhan, China, and a death toll of more than 1300K (World Health Organization, 2020). California is one of the most affected states in the United States (U.S.) partly because its poor air quality makes Californians more susceptible to infectious diseases such as COVID-19 (Bashir et al., 2020; Chiara Copat, 2020). In response to the emergence of COVID-19, statewide stay-at-home orders and related actions (e.g., closure of nonessential businesses) took effect on March 19, 2020 in California. These orders are expected to reduce vehicle traffic and industrial activities, thereby changing the air pollutant emissions and air quality in the state. It is essential to obtain a high-spatiotemporal-resolution estimation of air pollution for better understanding of the atmospheric impacts caused by changes in anthropogenic activity associated with the COVID-19 pandemic.

A number of studies emerged soon after the start of the COVID-19 pandemic and the subsequent lockdown to assess the impact of the pandemic on air quality over various regions around the world. For example, Archer et al. (2020) compared the observed concentrations at all available ground monitoring sites in U.S. between April of 2020 and the prior five years (2015–2019) and found statistically significant decreases in NO_2 concentrations at more than 65% of the monitoring sites, with an average drop of 2 ppb. Pan et al. (2020) compared the surface air quality monitoring data in California during the period 20 March–5 May in 2020 with those in 2015–2019 and found that the $PM_{2.5}$ in 2020 exhibited a notable decrease which could result from emission reductions associated with the COVID-19 lockdown. Similar findings, i.e., reduced $PM_{2.5}$ and NO_2 concentrations are also reported for China (e.g., Chu et al., 2020; Le et al., 2020; Liu et al., 2020; Marlier et al., 2020; Shi and Brasseur, 2020; Miyazaki et al., 2020b), India (e.g., Pathakoti et al., 2020; Sharma et al., 2020), and Europe (e.g., Chen et al., 2020; Menut et al., 2020; Sicard et al., 2020; Ordóñez et al., 2020) based on surface and/or satellite observations. For O_3, the concentrations either increased or slightly decreased during the pandemic, depending on regions (Bekbulat et al., 2020; Huang et al., 2020; Pan et al., 2020; Zhao et al., 2020). Most of the above studies, however, are

65 limited to comparing observations with and without lockdown measures, which correspond to different time periods under different meteorological conditions.

Meteorology plays significant roles in air pollution formation, transport, deposition and transformation (Wang et al., 2020a), which is a very important factor that affects concentrations of O_3 and $PM_{2.5}$ (Stewart et al., 2017). The changes in air quality due to meteorological variations may obscure the effects of emission changes during the COVID-19 lockdown. Using the

70 Community Multi-scale Air Quality model, Wang et al. (2020a) showed that the benefits of emission reductions were overwhelmed by adverse meteorology over the North China Plain and severe air pollution events were thus not avoided. Goldberg et al. (2020) reported that meteorological patterns were especially favorable for low NO_2 in much of the United States in spring 2020, complicating comparisons with spring 2019; the meteorological variations between years can cause ~15% difference in monthly mean column NO_2. In view of this, modelling approach is necessary to accurately assess the

75 impact of lockdown measures by excluding the possible effects of meteorological conditions and to examine the possible mechanisms responsible for the changes in the air pollutant concentrations. In addition, while previous studies have evaluated the air quality changes in different regions due to the emission reductions associated with the COVID-19 lockdown, it remains unclear how the COVID-19 induced emission reductions and the concurrent meteorological variations influence air quality in California.

80 The objective of this study is to investigate the air quality impact of the emission reductions in southern California in association with COVID-19 by employing high-resolution atmospheric modelling in combination with surface observations. Based on the statistics of activity levels together with constraints from satellite observations, we estimate the sectoral emission changes during the COVID-19 lockdown. We then conduct model simulations using the Weather Research and Forecasting model with Chemistry (WRF-Chem) for the periods before and during the COVID-19 lockdown to investigate

85 the effects of reduced emissions and meteorology on air pollution, respectively. Understanding how air quality responds to the emission reductions during COVID-19 pandemic will provide important insight into the future development and optimization of effective air pollution control strategies in southern California.

2 Method and Data

2.1 Model configuration and emission estimation

90 We simulate the impact of COVID-19 lockdown measures on air quality using the WRF-Chem version 3.9.1, which considers highly nonlinear and complex meteorological and atmospheric chemistry processes. The simulation period is February 18 to April 23, 2020, which includes about one month before and after the California governor issues the stay-at-home (lockdown) order on March 19 (Pan et al., 2020). We apply the model to two nested domains: Domain 1 covers the western United States and its surrounding areas at a 12 km×12 km horizontal resolution; Domain 2 covers California with a

95 4 km×4 km resolution (Fig. 1). We focus our analysis on southern California (the red rectangle in Fig. 1), the largest metropolitan area in California which is significantly affected by the lockdown measures. We classify model grids in

southern California into "urban" and "rural" areas to facilitate the analysis of O_3 simulation results. To be classified as "urban", an area in the U.S. needs to have a population density of 1,000 people per square mile (Ratcliffe et al., 2016), i.e., about 6000 people per 4 km×4 km model grid. As we focus our analysis on southern California, one of the most densely populated areas in the U.S., we use a higher population density threshold of 30,000 people per model grid to better distinguish areas with different photochemistry regimes (Fig. S1). We employ an extended Carbon Bond 2005 (CB05) (Yarwood et al., 2005) with chlorine chemistry (Sarwar et al., 2008) coupled with the Modal for Aerosol Dynamics in Europe/Volatility Basis Set (MADE/VBS) (Wang et al., 2015a; Ahmadov et al., 2012). MADE/VBS uses a modal aerosol size representation and an advanced secondary organic aerosol (SOA) module based on the VBS approach. The aqueous-phase chemistry is based on the AQChem module used in the Community Multiscale Air Quality (CMAQ) model (Wang et al., 2015a). The chemical initial and boundary conditions were extracted from the output of the Whole Atmosphere Community Climate Model (WACCM) (Marsh et al., 2013). A 6-day spin-up period is used to minimize the influence of initial conditions on simulation results. The vertical resolution, meteorological initial and boundary conditions, and physical options are the same as our previous modeling studies based on WRF-Chem for California (Zhao et al., 2019a; Wang et al., 2020b; Shi et al., 2019).

We obtain anthropogenic emissions in California without the influence of COVID-19 lockdown measures from the California Air Resources Board (CARB) for 2012 that is the latest year in which the data are available (California Air Resources Board, 2018). We scale the 2012 emissions to the 2020 levels by employing the relative changes for 2012–2018 in California from the "NEI trend report" (US Environmental Protection Agency, 2018a) and assuming that the trends continued during 2018–2020. The anthropogenic emissions outside California are derived from the National Emission Inventory (US Environmental Protection Agency, 2018b) in 2011 and are scaled to 2020 following the same method. The biogenic, wind-blown dust, sea-salt, and wildfire emissions are calculated online in WRF-Chem, as detailed in our previous studies (Zhao et al., 2019a; Wang et al., 2020b; Shi et al., 2019).

In our baseline simulation ("Base" scenario in Table 1), we use the above emission inventories. To evaluate the effect of the COVID-19 response actions, we conduct another simulation ("Lockdown" scenario in Table 1) in which the CARB anthropogenic emission inventory after March 19 is adjusted to account for the emission changes due to the COVID-19 lockdown. Because of the lack of detailed emission data which often take years to update, we rely on a number of key activity indicators to estimate the sector-specific relative changes in anthropogenic emissions (as summarized in Table 2), which are subsequently evaluated against satellite-derived emission estimate. For the transportation sector, we separately estimate the reduction rates for onroad, off-road, and aircraft emissions due to the COVID-19 lockdown. Specifically, we assume the reduction rates in gasoline and diesel vehicle emissions in the onroad sector to be the same as the reduction rates in gasoline and diesel production from the pre-lockdown period to the lockdown period, as documented by California Energy Commission's "Weekly Fuels Watch Reports" (California Energy Commission, 2020b). We then estimate the reduction rates in total emissions from the onroad sector based on the relative fractions of gasoline and diesel vehicle emissions reported by the CARB emission inventory. Since the off-road sector involves few gasoline vehicles, we assume the reduction rates in

4

off-road emissions to be the same as the reduction rate in diesel production. For the aircraft sector, we assume the reduction rates in aircraft emissions to be the same as the reduction rate in jet fuel production from the "Weekly Fuels Watch Reports" (California Energy Commission, 2020b). The changes in emissions from the industrial, residential, and commercial sectors are assumed to be proportional to the changes in electricity consumption by the corresponding sector, as summarized in the "Energy Insights Reports" of the California Energy Commission (California Energy Comission, 2020a). The changes in emissions from power plants are estimated as a function of the total electricity demand in California (California Energy Comission, 2020a). We also checked the emission change of power plants measured by the Continuous Emission Monitoring System (CEMS). There are certain differences between the emission reduction rates estimated based on the CESM and electricity demand, but the difference only results in a less than 1% difference in the total emissions of any pollutant (from 0.05% to 1%), which is expected to have a limited effect on the simulation results of mean air pollutant concentrations in southern California (see details in the Supplementary text and Fig. S3). Having estimated the emission changes using the preceding bottom-up method, in order to prove the reliability of our bottom-up emissions, we compare the changes in nitrogen oxides (NO_x) emissions with a top-down satellite-based emission inventory—an extended calculation of the Tropospheric Chemistry Reanalysis version 2 (TCR-2) (Miyazaki et al., 2020a). This data product has been obtained from the assimilation of multiple satellite measurements of ozone, CO, NO_2, HNO_3, and SO_2 from the OMI (Ozone Monitoring Instrument), TROPOMI (TROPOspheric Monitoring Instrument), MLS (Microwave Limb Sounder), and MOPITT (Measurement Of Pollution In The Troposphere) satellite instruments. The reanalysis calculation for the COVID-19 time period was conducted at 0.56° horizontal resolution using a global chemical transport model MIROC-CHASER (Watanabe et al., 2011) and an ensemble Kalman filter technique that optimizes chemical concentrations of various species and emissions of NO_x, SO_2, and CO. The extended reanalysis data for 2020 have already been used by Miyazaki et al. (2020b) to study air quality response to the Chinese COVID-19 lockdown measures. Here we use the NO_x emission product which has a sufficiently high quality on the spatiotemporal scales of interest for this study. Using this product, we first calculate NO_x emissions in a hypothetical scenario without considering the COVID-19 effect. Here the hypothetical emission trend in 2020 is averaged from those trends from the top-down NOx emission inventory in the prior years (2017-2019). We subsequently quantify the emission changes due to the COVID-19 using the difference between the hypothetical and real-world emissions (see details in Fig. 2). The estimated NO_x reduction ratio induced by the COVID-19 lockdown measures averaged during March 19 to April 23 in southern California is 27.2% based on the top-down method, which is in good agreement with the 28.3% (see Table 2) reduction estimated based on the bottom-up method. That said, we acknowledge that, since more detailed data to support a more accurate estimation are not yet available, the estimates of the sector-specific relative changes in emissions inevitably involve some degree of uncertainty, which can be improved in the future work.

2.2 Observational data and model evaluation

We use a series of meteorology and air quality observations to evaluate the model performance and help analyze the influence of the COVID-19 lockdown. For meteorology, we use observational data obtained from the National Climatic Data

Center (NCDC), where hourly or 3-hour observations of wind speed at 10 m (WS10), temperature at 2 m (T2), and water vapor mixing ratio at 2 m (Q2) are available for 82 sites distributed southern California (the red rectangle in Fig. 1). We compare the WRF-Chem meteorological simulations with these measurements and apply a number of statistical indices defined in Emery et al. (2001) to quantitatively evaluate the model performance, as summarized in Table 3. In general, the model simulations agree fairly well with surface meteorological observations. The performance statistics for WS10, T2 and Q2 are all within the benchmark ranges proposed by Emery et al. (2001).

For air quality, we achieve hourly observations of $PM_{2.5}$, O_3, NO_2 and SO_2 from CARB (California Air Resources Board, 2020) and use them to evaluate the air quality simulations of WRF-Chem (see the Results and Discussion section). The observational data are available at 42 sites for $PM_{2.5}$, 63 sites for O_3, 48 sites for NO_2, and 12 sites for SO_2, in southern California (the red rectangle in Fig. 1) during the simulation period. We do not evaluate the model performance in simulating the chemical composition of $PM_{2.5}$ because the composition data from major observational networks had not been available by the time we completed the present study. Nevertheless, our previous studies using almost the same model configurations showed a fairly good agreement with $PM_{2.5}$ composition observations during January, April, July, and October, 2012 (Zhao et al., 2019a; Wang et al., 2020b).

3 Results and Discussion

3.1 Evaluation of the simulated results with surface observations

In this study, we simulated the major air pollutants using WRF-Chem under two scenarios, Base and Lockdown (Table 1). To evaluate the model performance with regard to the temporal variations in air pollutants, we compared the simulated concentrations of $PM_{2.5}$, maximum daily 8-h average (MDA8) O_3, NO_2 and SO_2 with observational data from CARB in southern California.

Before the COVID-19 lockdown (February 18 to March 18), results from model simulation under the Base scenario (Pre_{Base}) capture the magnitude and temporal evolution of the four key air pollutants reasonably well, with normalize mean biases (NMBs) of 11.7%, 4.5%, -14.4% and 7.8% for $PM_{2.5}$, MDA8 O_3, NO_2, SO_2, respectively (Fig. 3). During the COVID-19 lockdown period (March 19 to April 23), compared to the simulations for the Base scenario ($Post_{Base}$) which overestimates the surface concentrations with NMBs of 28.1%, 1.6%, 21.4% and 39.2% for $PM_{2.5}$, MDA8 O_3, NO_2, SO_2, respectively, the simulated results using the adjusted emission inventory ($Post_{Lockdown}$) not only agree better with surface observations for all the four air pollutants (with NMBs of 10.6%, 1.0%, -12.6% and -13.1% for $PM_{2.5}$, MDA8 O_3, NO_2, SO_2, respectively), but also show generally closer NMBs to those during the pre-lockdown period (Fig. 3). The improvement in model performance is observed for both urban and rural areas. In the urban areas, the NMB for $PM_{2.5}$ drops from 25.8% under the Base scenario to 3.9% under the Lockdown scenario, getting closer to the NMB of 4.0% during the pre-lockdown period. The corresponding NMB in rural areas drops from 29.7% to 15.1%, also getting closer to 17.8% during the pre-lockdown period (Figs. 3e,g). Regarding MDA8 O_3, although the differences between the Base and Lockdown scenarios are quite small (Fig.

6

3b), the NMB is slightly improved from -1.5% ($Post_{Base}$) to -0.2% ($Post_{Lockdown}$) in urban areas and from 3.2% to 1.5% in rural areas (Figs. 3f,h).

Subsequently, we evaluated the spatial distributions of simulated $PM_{2.5}$ and MDA8 O_3 concentrations using observational data averaged during the pre-lockdown and lockdown periods in southern California (Fig. 4). Figure S4 shows the scattergrams of the simulated and observed monthly average $PM_{2.5}$ and MDA8 O_3 concentrations in southern California. The Base scenario can simulate the spatial patterns of $PM_{2.5}$ and MDA8 O_3 reasonably well (Figs. 4a-b and d-e), but it overestimates the observations of $PM_{2.5}$ concentrations during the lockdown period ($Post_{Base}$, Figs. 4b and S4b). The simulated distributions of $PM_{2.5}$ concentrations under the Lockdown scenario ($Post_{Lockdown}$) match the observations better than those for the Base scenario ($Post_{Base}$) (Figs. 4b-c and S4b-c); the hot spots occurring over the Los Angeles County become less polluted and more consistent with the surface observations after considering the emission reductions associated with the COVID-19 lockdown (Figs. 4b-c).

3.2 Effects of anthropogenic emission reductions and meteorology conditions on air pollutants

Both observations and simulations in Fig. 3 show significant changes in air pollutant concentrations during the COVID-19 lockdown relative to the pre-lockdown period, resulting from a combination of emission reductions and meteorology variations. Our model simulations allow us to quantify the relative contributions of these two factors. Figures 5a-f illustrate population-weighted concentrations of simulated $PM_{2.5}$ components, NO_2, SO_2, MDA8 O_3 in southern California, and MDA8 O_3 over the urban and rural areas of southern California under the Base and Lockdown scenarios. We use population-weighted concentrations because they are more relevant to the health impacts of air pollutants ($PM_{2.5}$ and O_3), the mitigation of which is an ultimate goal of controlling air pollution. Figure S5 shows the mean concentrations of simulated $PM_{2.5}$ components, MDA8 O_3, NO_2, and SO_2 in southern California.

The simulations of the Base and Lockdown scenarios during the lockdown period ($Post_{Base}$ and $Post_{Lockdown}$) have the same model configurations and inputs (same large-scale meteorological conditions) except for different emission inventories. The concentration differences between the two scenarios during the lockdown period ($Post_{Lockdown}$−$Post_{Base}$) represent the effect of anthropogenic emission reductions. Strictly speaking, while the large-scale meteorological fields are the same in $Post_{Base}$ and $Post_{Lockdown}$, the different emission inputs could cause small differences in regional meteorology fields through the interactions between air pollutants and meteorology. Such a meteorology perturbation is considered to be part of the emission reduction effect because it is fundamentally caused by emission reductions. The simulations of the Base scenario during the lockdown and pre-lockdown periods ($Post_{Base}$ and Pre_{Base}) both use the emission inventories without considering the COVID-19 induced emission reductions. The differences between $Post_{Base}$ and Pre_{Base} can be regarded as the impact of meteorology variations. Here our intention is to examine the relative contribution of meteorological variations to the population-weighted air pollutant concentrations before and after the lockdown, instead of the changes relative to the climatological conditions. However, we acknowledge that it is more meaningful and informative to assess the meteorological effect by conducting ensemble simulations over multiple years or use multi-year averaged meteorological conditions to serve

as a reference state (Le et al., 2020), which warrants further studies in the future. Figures 6 and 7 further show the spatial

230 distribution of the concentration changes caused by anthropogenic emission reductions and meteorology variations.

The simulated population-weighted NO_2 concentrations during the lockdown decrease by 4.3 ppb (from 10.7 to 6.4 ppb) relative to the pre-lockdown period, of which the anthropogenic emission reductions and meteorology conditions contribute 2.4 ppb (56%) and 1.9 ppb (44%), respectively (Fig. 5b). The decrease in NO_2 concentrations as a result of the anthropogenic emission reductions (27%) is similar to the reduction ratio in NO_x emission (28%), indicating that the NO_x emission

235 reductions can be almost fully transferred to ambient concentrations. According to our emission estimation, over 80% of the NO_x reductions is attributed to the substantially lowered traffic intensity due to the stay-at-home order. Note that the soil NO_x emissions are not taken into account in our WRF-Chem simulation. According to Guo et al. (2020), the total soil NO_x emissions in California account for only about 1.1% of the state's total anthropogenic NO_x emissions (California Air Resources Board, 2017). The soil NO_x emissions in southern California are even generally lower compared with other parts

240 of the state (Guo et al., 2020). Since our study focuses on the impact of anthropogenic emission reductions on air quality during the COVID-19 lockdown period, the absence of soil NO_x emissions has little impact on our main results and will not change the main findings of this study. The population-weighted concentrations of SO_2 also show a decreasing trend (Fig. 5c). Compared with NO_2, the decrease in SO_2 concentrations due to emission reductions is smaller (17%), partly because power generators and heavy industry (the main sources of SO_2) are less affected by the COVID-19 lockdown (see Table 2).

245 Coinciding with the decrease in NO_2 and SO_2, the simulated population-weighted $PM_{2.5}$ concentrations decrease by 1.8 $\mu g/m^3$ from 8.7 $\mu g/m^3$ during the pre-lockdown period (Pre_{Base}) to 6.9 $\mu g/m^3$ during the lockdown period ($Post_{Lockdown}$). The emission reductions contribute 1.2 $\mu g/m^3$ (67%) of the above decrease, which translates into a 15% reduction in population-weighted $PM_{2.5}$ concentrations from the levels without the lockdown (i.e., $Post_{Base}$) (Fig. 5a). The decrease occurs almost everywhere across the domain (Fig. 6a), consistent with the results in the last section that $PM_{2.5}$ concentrations are lowered

250 in both urban and rural areas as a result of the emission reductions (Figs. 3e,g). The concentration decrease is higher in urban areas than in rural areas (Figs. 6a and 3e,g), with the most significant decline occurring in urban areas of the Los Angeles County (Fig. 6a). In contrast, the meteorology variations can increase the $PM_{2.5}$ concentrations in some regions (mainly the inland regions) and decrease them in others (mainly the coastal regions) (Fig. 6b). The net effect is to reduce the population-weighted concentration by 0.6 $\mu g/m^3$ since the concentration decrease happens to occur in more densely populated regions

255 (Fig. 5a).

The concentrations of $PM_{2.5}$ are affected by emissions of multiple pollutants through both primary emissions and chemical reactions. To further explore the reasons behind the $PM_{2.5}$ concentration changes, we examine the changes in individual chemical components, as shown in Fig. 5a and Fig. 7. Following the emission changes (from $Post_{Base}$ to $Post_{Lockdown}$), all major $PM_{2.5}$ components experience a concentration decrease almost throughout the domain (Fig. 7), since the emissions of

260 essentially all pollutants are reduced to some extent due to the lockdown measures (Table 2). The population-weighted concentrations of nitrate decrease the most (0.42 $\mu g/m^3$), followed by "Others" (0.32 $\mu g/m^3$, including all other components besides the key components listed here), organic matter (OM, 0.16 $\mu g/m^3$), ammonium (0.15 $\mu g/m^3$), black carbon (BC, 0.10

μg/m^3), and sulfate (from 0.07 μg/m^3) (Fig. 5a). The largest decrease in nitrate is tied to the substantial reduction in NO$_x$ emissions, which is further explained by a larger reduction ratio in transportation emissions (by 30–70%) compared with other emission sources (Table 2). In addition, the decreases in "Others", EC, and primary OM (a fraction of the total OM) are attributable to the reductions in primary PM$_{2.5}$ emissions. In our emission estimates, the sector-specific relative emission changes of EC, primary OM, and "Others" are assumed to be the same as the total primary PM$_{2.5}$, as summarized in Table 2. For the total emissions of all sectors, the reduction in EC, primary OM, and "Others" are 22.7%, 15.8%, and 13.5%, respectively, slightly different from the reduction in total primary PM$_{2.5}$ since different chemical components have different sectoral distributions. The overall concentration decrease in these primary chemical components even exceeds that of nitrate; this clearly indicates an important role of primary PM$_{2.5}$ components in improving PM$_{2.5}$ air quality during the lockdown period, although the primary PM$_{2.5}$ emissions have only been reduced by 15%.

The simulated population-weighted O$_3$ concentrations increase noticeably from 38 ppb in the pre-lockdown period (Pre$_{Base}$) to 42 ppb (Post$_{Lockdown}$) during the lockdown, and the effects of meteorological changes (i.e. Post$_{Base}$−Pre$_{Base}$) play a dominant role in the variation of O$_3$. The O$_3$ level is strongly affected by ambient conditions like temperature and solar radiation (Wang et al., 2015b). As the temperature gets warmer and the radiation gets stronger over time, the O$_3$ concentrations are elevated in most areas during the COVID-19 lockdown, compared to the pre-lockdown period (Fig. 6d). The emission reductions cause an O$_3$ decrease in rural areas but a slight increase in the urban areas (Fig. 6c and Figs. 3f,h), which is consistent with previous findings (Zhao et al., 2019a; Wang et al., 2020b; Martien et al., 2003; Qin et al., 2004). In urban areas where NO$_x$ emissions are high, a volatile organic compounds (VOC)-limited regime is seen, while in rural areas, a NO$_x$-limited regime is observed (Martien et al., 2003; Qin et al., 2004). It follows that the decrease in NO$_x$ emissions leads to opposite changes in O$_3$ concentrations in urban and rural areas. The increase and decrease in different areas largely offset each other, resulting in a negligible change in population-weighted O$_3$ concentrations (0.07 ppb) (Fig. 5d) and a slight decrease in area-averaged O$_3$ concentrations over the modelling domain (0.77 ppb) (Figs. 6c and S5b). Last but not least, the small sensitivity of O$_3$ to emission reductions is also partly explained by the fact that 75% of the ambient O$_3$ concentration is background O$_3$ (Zhao et al., 2019a; Wang et al., 2020b).

3.3 Effects of anthropogenic NO$_x$ and VOC emission reductions on ozone concentration

Our modelling results showed an increase in O$_3$ in urban areas due to the emission reductions in association with the lockdown during the COVID-19 pandemic. The O$_3$ concentrations are most significantly affected by emissions of NO$_x$ and VOC (Stewart et al., 2017). To further explore the drivers of the O$_3$ changes and potential approaches to effectively reduce O$_3$ concentrations, we conduct three sensitivity experiments involving NOx and VOC emission perturbations, as summarized in Table 1. Figure 8 illustrates population-weighted concentrations of simulated PM$_{2.5}$ components and MDA8 O$_3$ after the COVID-19 lockdown under these sensitivity scenarios. Figure 9 shows the spatial distribution of the differences in MDA8 O$_3$ between the sensitivity scenarios and the Base scenario. The first sensitivity experiment is the VOC1.0 scenario which is

295   the same as "Lockdown" except that the VOC emissions are kept at the level of the "Base" scenario (Table 1). This scenario, in combination with the Base and Lockdown scenarios, can be used to evaluate the response of O_3 concentrations if the COVID-19 induced emission reductions of NO_x and VOC were implemented in sequence. Without the control of VOC emissions in VOC1.0 (Fig. 9a), the increase in urban O_3 concentration relative to the Base scenario becomes larger than the Lockdown scenario (Fig. 6c). This confirms our analysis in the last section that the NO_x emission control elevates urban O_3

300   concentrations under the VOC-limited regime and meanwhile indicates that the VOC control is conducive to O_3 decrease. To assess the potential effects of strengthened NO_x and VOC control measures, we conduct two other sensitivity experiments named $NO_x0.3$ and VOC0.3, which are the same as "Lockdown" except that the anthropogenic NO_x (for the $NO_x0.3$ scenario) and VOC (for the VOC0.3 scenario) emissions are further reduced to 30% of those in the "Base" scenario. As a 70% reduction is close to the maximum reductions in NO_x and VOC emissions that could be achieved through the full

305   implementation of technologically and economically feasible control measures (Amann et al., 2020), we select an emission ratio of 0.3 (70% reduction) to represent the potential impact of highly stringent control policies in the future. Figs. 8a,b show that strengthened NO_x control further reduces the population-weighted concentrations of $PM_{2.5}$, while further reduction of anthropogenic VOC helps to decrease the concentration of MDA8 O_3. Differences in O_3 concentration clearly illustrate different spatial distribution patterns for urban and suburb areas (Figs. 9b, c). For the suburbs with high O_3 values, reducing

310   anthropogenic NO_x and VOC is conducive to the decline of O_3 (Fig. 8d). For urban areas, however, strengthened control with anthropogenic NO_x reduced by 70% ($NO_x0.3$) results in even more O_3 increase in the central urban area (Figs. 9b and 8c). Amplified ozone pollution has also been reported by Sicard et al. (2020) based on their observational studies in four Southern European cities and Wuhan, China associated with NO_x reductions in response to COVID-19. To control O_3 concentrations in urban areas, VOC control may be an effective method. While a NO_x emission reduction might cause an

315   increase in O_3 concentration, a VOC reduction generally leads to a monotonous reduction of O_3 concentrations regardless of the O_3 formation regime, as indicated by the classical O_3 EKMA isopleth (Figure 6-1 of National Research Council (1991) or Figure 3.2.1 of Donahue (2018)) as well as some recent studies in southern California (Fujita et al., 2013; Collet et al., 2018; Qian et al., 2019). We find that in the VOC0.3 scenario, there is almost no O_3 concentration increase relative to the Base scenario, in contrast to a significant urban O_3 increase in the Lockdown scenario (Fig. 9c). This means that a 70% reduction

320   in anthropogenic VOC can offset the increases in O_3 caused by the 28.3% NO_x reduction during the lockdown. Note that we are specifically looking at the extent of VOC emission reductions that are needed to offset the 28.3% NO_x reduction caused by the lockdown, which minimizes the complexity due to the nonlinear O_3 responses when the NO_x emissions are changing simultaneously. Furthermore, Wang et al. (2019) found that 75% of the average O_3 concentration in California was due to distant emissions outside the western United States. Many other studies also revealed that the background O_3 dominates over

325   the contribution from local emissions in the western U.S. (Huang et al., 2015; Oltmans et al., 2008; Fiore et al., 2014; Emery et al., 2012; Zhang et al., 2011). Therefore, cooperating with other regions and countries in emission reductions may be another way to control O_3 in urban areas of the southern California.

4 Conclusion and policy implications

In this study, we investigated the air quality impact of the emission reductions in southern California in association with COVID-19 by employing WRF-Chem to conduct high-resolution atmospheric modeling during February 18 to April 23, 2020.

Based on the statistics of activity levels, we first adjusted the emission inventory considering the emission reductions during the COVID-19 lockdown. The adjusted emission inventory is shown to be consistent with the emission inventory based on satellite observations. The simulated magnitude and temporal evolution of the concentrations of the key air pollutants, including $PM_{2.5}$, NO_2, SO_2, and MDA8 O_3 using the adjusted emission inventory agree better with surface observations than simulation results without considering the COVID-19 induced emission reductions. Due to the reduced emissions, the population-weighted concentrations of NO_2 and $PM_{2.5}$ decreased by 27% and 15%, respectively, in southern California in the five weeks after the stay-at-home orders. Emission reductions and meteorological variations contributed about two-thirds and one-third, respectively, to the total decrease in population-weighted $PM_{2.5}$ concentrations before and after the lockdown.

For O_3 concentration, however, the COVID-19 related emission reductions caused a decrease in suburb areas but a slight increase in the urban areas. In order to further explore the effects of anthropogenic NO_x and VOC emission reductions on O_3 concentration, we conducted sensitivity experiments by strengthening VOC and NO_x controls. Our results showed that strengthened control with NO_x reduced by 70% ($NO_x0.3$) results in even more O_3 increase in the central urban area and anthropogenic VOC control may be an effective method to reduce O_3 concentrations in urban areas. A 70% reduction in anthropogenic VOC can effectively offset all the increases in O_3 caused by NO_x reduction during the lockdown.

Using the COVID-19 as an unprecedented experiment with substantial emission reductions from multiple sectors, especially transportation, this study helps to elucidate the complex and nonlinear response of chemical compositions to air pollution control measures and thus provides important insight into the development and optimization of effective air pollution control strategies in southern California. We find that the reduced NO_x emission (~28%) has been almost fully transferred to the reduction in ambient concentration of NO_2 (~27%). This further translates into a remarkable reduction in nitrate, which makes the largest contribution to $PM_{2.5}$ concentration decrease among all individual chemical components. Therefore, to alleviate the $PM_{2.5}$ pollution, measures focusing on sectors such as transportation, which is among the main sources of NO_x emission, could be effective. Moreover, we find that a moderate 15% reduction of primary $PM_{2.5}$ emissions has resulted in a substantial reduction in ambient $PM_{2.5}$ concentrations, with the total concentration decreases in all primary $PM_{2.5}$ components exceeding that of nitrate. Therefore, a strengthened control on primary $PM_{2.5}$ emissions could be an effective strategy to sustainably mitigate $PM_{2.5}$ pollution. For O_3, reduction of NO_x can effectively reduce the high O_3 concentrations in suburban areas, but may cause an increase of urban concentrations. A 70% VOC emission reduction is found to fully offset the urban O_3 increase caused by the lockdown. Therefore, the reduction in NO_x emissions needs to be accompanied by a well-balanced reduction in VOC emissions to avoid the side effect on urban O_3 pollution.

Data Availability Statement

Acknowledgments

**References**

Ahmadov, R., McKeen, S. A., Robinson, A. L., Bahreini, R., Middlebrook, A. M., de Gouw, J. A., Meagher, J., Hsie, E. Y., Edgerton, E., Shaw, S., and Trainer, M.: A volatility basis set model for summertime secondary organic aerosols over the eastern United States in 2006, J Geophys Res-Atmos, 117, D06301, DOI 10.1029/2011jd016831, 2012.

Amann, M., Kiesewetter, G., Schöpp, W., Klimont, Z., Winiwarter, W., Cofala, J., Rafaj, P., Höglund-Isaksson, L., Gomez-Sabriana, A., and Heyes, C.: Reducing global air pollution: the scope for further policy interventions, Philosophical Transactions of the Royal Society A, 378, 20190331, 2020.

Archer, C. L., Cervone, G., Golbazi, M., Fahel, N. A., and Hultquist, C.: Changes in air quality and human mobility in the US during the COVID-19 pandemic, arXiv preprint arXiv:2006.15279, 2020.

Bashir, M. F., Bilal, B. M., and Komal, B.: Correlation between environmental pollution indicators and COVID-19 pandemic: A brief study in Californian context, Environmental Research, 109652, 2020.

Bekbulat, B., Apte, J. S., Millet, D. B., Robinson, A., Wells, K. C., and Marshall, J. D.: PM2. 5 and Ozone Air Pollution Levels Have Not Dropped Consistently Across the US Following Societal Covid Response, 2020.

California Air Resources Board (2018), CEPAM: Emission Projections By Summary Category: : https://www.arb.ca.gov/app/emsinv/fcemssumcat/fcemssumcat2016.php, access: October 1st, 2018.

395 California Air Resources Board (2017), Emission Inventory Data. 2012 Base Year Emissions. Sacramento, California. Available at: https://ww3.arb.ca.gov/ei/emissiondata.htm, access: July 5th, 2018.

California Air Resources Board (2020), Air Quality Data: https://www.arb.ca.gov/aqmis2/aqdselect.php, access: May 19, 2020.

California Energy Comission, Energy Insights: : https://www.energy.ca.gov/data-reports/energy-insights, access: July 1st,
400 2020a.

California Energy Commission, Weekly Fuels Watch Report: https://ww2.energy.ca.gov/almanac/petroleum_data/fuels_watch/index_cms.html, access: July 1st, 2020b.

Chen, D., Li, Q., Stutz, J., Mao, Y., Zhang, L., Pikelnaya, O., Tsai, J. Y., Haman, C., Lefer, B., and Rappenglück, B.: WRF-Chem simulation of NOx and O3 in the LA basin during CalNex-2010, Atmospheric Environment, 81, 421-432, 2013.

405 Chen, L.-W. A., Chien, L.-C., Li, Y., and Lin, G.: Nonuniform impacts of COVID-19 lockdown on air quality over the United States, Science of The Total Environment, 141105, 2020.

Chiara Copat, A. C., Maria Fiora, Alfina Grasso, Pietro Zuccarello, Salvatore Santo Signorelli, Gea Oliveri Conti, Margherita Ferrante: The role of air pollution (PM and NO2) in COVID-19 spread and lethality: a systematic review, 191, https://doi.org/10.1016/j.envres.2020.110129, 2020.

410 Chu, B., Zhang, S., Liu, J., Ma, Q., and He, H.: Significant concurrent decrease in PM2. 5 and NO2 concentrations in China during COVID-19 epidemic, Journal of Environmental Sciences, 2020.

Collet, S., Kidokoro, T., Karamchandani, P., and Shah, T.: Future-year ozone isopleths for South Coast, San Joaquin Valley, and Maryland, Atmosphere, 9, 354, 2018.

Donahue, N. M.: Chapter 3.2 - Air pollution and air quality, in: Green Chemistry, Elsevier, 151-176, 2018.

415 Emery, C., Tai, E., and Yarwood, G.: Enhanced meteorological modeling and performance evaluation for two texas episodes. Report to the Texas Natural Resources Conservation Commission, ENVIRON International Corporation, Novato, CA, 2001.

Emery, C., Jung, J., Downey, N., Johnson, J., Jimenez, M., Yarvvood, G., and Morris, R.: Regional and global modeling estimates of policy relevant background ozone over the United States, Atmospheric Environment, 47, 206-217,
420 10.1016/j.atmosenv.2011.11.012, 2012.

Fiore, A. M., Oberman, J. T., Lin, M. Y., Zhang, L., Clifton, O. E., Jacob, D. J., Naik, V., Horowitz, L. W., Pinto, J. P., and Milly, G. P.: Estimating North American background ozone in U.S. surface air with two independent global models: Variability, uncertainties, and recommendations, Atmospheric Environment, 96, 284-300, 10.1016/j.atmosenv.2014.07.045, 2014.

425 Fujita, E. M., Campbell, D. E., Stockwell, W. R., and Lawson, D. R.: Past and future ozone trends in California's South Coast Air Basin: Reconciliation of ambient measurements with past and projected emission inventories, Journal of the Air & Waste Management Association, 63, 54-69, 2013.

Goldberg, D. L., Anenberg, S. C., Griffin, D., McLinden, C. A., Lu, Z., and Streets, D. G.: Disentangling the impact of the COVID‐19 lockdowns on urban NO2 from natural variability, Geophysical Research Letters, e2020GL089269, 2020.

430 Guo, L., Chen, J., Luo, D., Liu, S., Lee, H. J., Motallebi, N., Fong, A., Deng, J., Rasool, Q. Z., and Avise, J. C.: Assessment of Nitrogen Oxide Emissions and San Joaquin Valley PM2. 5 Impacts From Soils in California, Journal of Geophysical Research: Atmospheres, 125, e2020JD033304, 2020.

Hong, A., Schweitzer, L., Yang, W., and Marr, L. C.: Impact of temporary freeway closure on regional air quality: a lesson from Carmageddon in Los Angeles, United States, Environmental Science & Technology, 49, 3211-3218, 2015.

435 Huang, M., Bowman, K. W., Carmichael, G. R., Lee, M., Chai, T. F., Spak, S. N., Henze, D. K., Darmenov, A. S., and da Silva, A. M.: Improved western US background ozone estimates via constraining nonlocal and local source contributions using Aura TES and OMI observations, J Geophys Res-Atmos, 120, 3572-3592, 10.1002/2014jd022993, 2015.

Huang, X., Ding, A., Gao, J., Zheng, B., Zhou, D., Qi, X., Tang, R., Wang, J., Ren, C., and Nie, W.: Enhanced secondary pollution offset reduction of primary emissions during COVID-19 lockdown in China, National Science Review, 2020.

440 Le, T., Wang, Y., Liu, L., Yang, J., Yung, Y. L., Li, G., and Seinfeld, J. H.: Unexpected air pollution with marked emission reductions during the COVID-19 outbreak in China, Science, 369, 702-706, 2020.

Liu, F., Page, A., Strode, S. A., Yoshida, Y., Choi, S., Zheng, B., Lamsal, L. N., Li, C., Krotkov, N. A., and Eskes, H.: Abrupt decline in tropospheric nitrogen dioxide over China after the outbreak of COVID-19, Science Advances, eabc2992, 2020.

Marlier, M. E., Xing, J., Zhu, Y., and Wang, S.: Impacts of COVID-19 response actions on air quality in China,

445   Environmental Research Communications, 2, 075003, 10.1088/2515-7620/aba425, 2020.

Marsh, D. R., Mills, M. J., Kinnison, D. E., Lamarque, J. F., Calvo, N., and Polvani, L. M.: Climate Change from 1850 to 2005 Simulated in CESM1(WACCM), J Climate, 26, 7372-7391, 10.1175/jcli-d-12-00558.1, 2013.

Martien, P. T., Harley, R. A., Milford, J. B., and Russell, A. G.: Evaluation of incremental reactivity and its uncertainty in southern California, Environmental science & technology, 37, 1598-1608, 2003.

450   Menut, L., Bessagnet, B., Siour, G., Mailler, S., Pennel, R., and Cholakian, A.: Impact of lockdown measures to combat Covid-19 on air quality over western Europe, Science of The Total Environment, 741, 140426, 2020.

Miyazaki, K., Bowman, K., Sekiya, T., Eskes, H., Boersma, F., Worden, H., Livesey, N., Payne, V. H., Sudo, K., Kanaya, Y., Takigawa, M., and Ogochi, K.: An updated tropospheric chemistry reanalysis and emission estimates, TCR-2, for 2005–2018, Earth System Science Data Discussions, DOI 10.5194/essd-2020-30, 2020a.

455   Miyazaki, K., Bowman, K., Sekiya, T., Jiang, Z., Chen, X., Eskes, H., Ru, M., Zhang, Y., and Shindell, D.: Air Quality Response in China Linked to the 2019 Novel Coronavirus (COVID‐19) Lockdown, Geophysical research letters, 47, e2020GL089252, 2020b.

National Research Council. Rethinking the Ozone Problem in Urban and Regional Air Pollution. Washington, DC: The National Academies Press, https://doi.org/10.17226/1889, 1991.

460   Oltmans, S. J., Lefohn, A. S., Harris, J. M., and Shadwick, D. S.: Background ozone levels of air entering the west coast of the US and assessment of longer-term changes, Atmospheric Environment, 42, 6020-6038, 10.1016/j.atmosenv.2008.03.034, 2008.

Ordóñez, C., Garrido-Perez, J. M., and García-Herrera, R.: Early spring near-surface ozone in Europe during the COVID-19 shutdown: Meteorological effects outweigh emission changes, Science of The Total Environment, 141322, 2020.

465   Pan, S., Jung, J., Li, Z., Hou, X., Roy, A., Choi, Y., and Gao, H. O.: Air Quality Implications of COVID-19 in California, Sustainability, 12, 7067, 2020.

Pathakoti, M., Muppalla, A., Hazra, S., Dangeti, M., Shekhar, R., Jella, S., Mullapudi, S. S., Andugulapati, P., and Vijayasundaram, U.: An assessment of the impact of a nation-wide lockdown on air pollution–a remote sensing perspective over India, Atmospheric Chemistry and Physics Discussions, 1-16, 2020.

470   Qian, Y., Henneman, L. R., Mulholland, J. A., and Russell, A. G.: Empirical development of ozone isopleths: Applications to Los Angeles, Environmental Science & Technology Letters, 6, 294-299, 2019.

Qin, Y., Tonnesen, G., and Wang, Z.: One-hour and eight-hour average ozone in the California South Coast air quality management district: trends in peak values and sensitivity to precursors, Atmospheric Environment, 38, 2197-2207, 2004.

Ratcliffe, M., Burd, C., Holder, K., and Fields, A.: Defining rural at the US Census Bureau, American community survey and
475   geography brief, 1, 2016.

Sarwar, G., Luecken, D., Yarwood, G., Whitten, G. Z., and Carter, W. P. L.: Impact of an updated carbon bond mechanism on predictions from the CMAQ modeling system: Preliminary assessment, J Appl Meteorol Clim, 47, 3-14, 10.1175/2007jamc1393.1, 2008.

Sharma, S., Zhang, M., Gao, J., Zhang, H., and Kota, S. H.: Effect of restricted emissions during COVID-19 on air quality in
480   India, Science of the Total Environment, 728, 138878, 2020.

Shi, H. R., Jiang, Z., Zhao, B., Li, Z. J., Chen, Y., Gu, Y., Jiang, J. H., Lee, M., Liou, K. N., Neu, J. L., Payne, V. H., Su, H., Wang, Y., Witek, M., and Worden, J.: Modeling Study of the Air Quality Impact of Record-Breaking Southern California Wildfires in December 2017, J Geophys Res-Atmos, 124, 6554-6570, 10.1029/2019jd030472, 2019.

Shi, X., and Brasseur, G. P.: The Response in Air Quality to the Reduction of Chinese Economic Activities during the
485   COVID‐19 Outbreak, Geophysical Research Letters, e2020GL088070, 2020.

Shirmohammadi, F., Hasheminassab, S., Saffari, A., Schauer, J. J., Delfino, R. J., and Sioutas, C.: Fine and ultrafine particulate organic carbon in the Los Angeles basin: Trends in sources and composition, Science of The Total Environment, 541, 1083-1096, 2016.

Sicard, P., De Marco, A., Agathokleous, E., Feng, Z., Xu, X., Paoletti, E., Rodriguez, J. J. D., and Calatayud, V.: Amplified
490   ozone pollution in cities during the COVID-19 lockdown, Science of The Total Environment, 139542, 2020.

Stewart, D. R., Saunders, E., Perea, R. A., Fitzgerald, R., Campbell, D. E., and Stockwell, W. R.: Linking air quality and human health effects models: an application to the Los angeles air basin, Environmental health insights, 11, 1178630217737551, 2017.

US Environmental Protection Agency, Air Pollutant Emissions Trends Data: https://www.epa.gov/air-emissions-

inventories/air-pollutant-emissions-trends-data, access: December 10th, 2018, 2018a.

US Environmental Protection Agency, National Emissions Inventory (NEI): https://www.epa.gov/air-emissions-inventories/national-emissions-inventory-nei, access: December 10th, 2018, 2018b.

Wang, K., Zhang, Y., Yahya, K., Wu, S. Y., and Grell, G.: Implementation and initial application of new chemistry-aerosol options in WRF/Chem for simulating secondary organic aerosols and aerosol indirect effects for regional air quality, Atmos Environ, 115, 716-732, 10.1016/j.atmosenv.2014.12.007, 2015a.

Wang, P., Chen, K., Zhu, S., Wang, P., and Zhang, H.: Severe air pollution events not avoided by reduced anthropogenic activities during COVID-19 outbreak, Resources, Conservation and Recycling, 158, 104814, 2020a.

Wang, T., Zhao, B., Liou, K.-N., Gu, Y., Jiang, Z., Song, K., Su, H., Jerrett, M., and Zhu, Y.: Mortality burdens in California due to air pollution attributable to local and nonlocal emissions, Environment international, 133, 105232, 2019.

Wang, T. Y., Jiang, Z., Zhao, B., Gu, Y., Liou, K. N., Kalandiyur, N., Zhang, D., and Zhu, Y. F.: Health co-benefits of achieving sustainable net-zero greenhouse gas emissions in California, Nature Sustainability, 10.1038/s41893-020-0520-y, 2020b.

Wang, Z., Li, Y., Chen, T., Zhang, D., Sun, F., Wei, Q., Dong, X., Sun, R., Huan, N., and Pan, L.: Ground-level ozone in urban Beijing over a 1-year period: Temporal variations and relationship to atmospheric oxidation, Atmospheric Research, 164, 110-117, 2015b.

Warneke, C., De Gouw, J. A., Edwards, P. M., Holloway, J. S., Gilman, J. B., Kuster, W. C., Graus, M., Atlas, E., Blake, D., and Gentner, D. R.: Photochemical aging of volatile organic compounds in the Los Angeles basin: Weekday‐weekend effect, Journal of Geophysical Research: Atmospheres, 118, 5018-5028, 2013.

Watanabe, S., Hajima, T., Sudo, K., Nagashima, T., Takemura, T., Okajima, H., Nozawa, T., Kawase, H., Abe, M., Yokohata, T., Ise, T., Sato, H., Kato, E., Takata, K., Emori, S., and Kawamiya, M.: MIROC-ESM 2010: model description and basic results of CMIP5-20c3m experiments, Geosci Model Dev, 4, 845-872, 10.5194/gmd-4-845-2011, 2011.

WHO Coronavirus Disease (COVID-19) Dashboard: https://www.who.int/emergencies/diseases/novel-coronavirus-2019/situation-reports/, access: November 13, 2020, 2020.

Yarwood, G., Rao, S., Yocke, M., and Whitten, G. Z.: Final Report-updates to the Carbon Bond Chemical Mechanism: CB05 (RT-04-00675), Yocke and Co., Novato, California, 246, 2005.

Zhang, L., Jacob, D. J., Downey, N. V., Wood, D. A., Blewitt, D., Carouge, C. C., van Donkelaar, A., Jones, D. B. A., Murray, L. T., and Wang, Y. X.: Improved estimate of the policy-relevant background ozone in the United States using the GEOS-Chem global model with 1/2 degrees x 2/3 degrees horizontal resolution over North America, Atmospheric Environment, 45, 6769-6776, 10.1016/j.atmosenv.2011.07.054, 2011.

Zhao, B., Wang, S., Xing, J., Fu, K., Fu, J., Jang, C., Zhu, Y., Dong, X., Gao, Y., and Wu, W.: Assessing the nonlinear response of fine particles to precursor emissions: development and application of an extended response surface modeling technique v1. 0, Geoscientific Model Development (Online), 8, 115-128, 2015.

Zhao, B., Wan, T. Y., Jiang, Z., Gu, Y., Liou, K. N., Kalandiyur, N., Gao, Y., and Zhu, Y. F.: Air Quality and Health Cobenefits of Different Deep Decarbonization Pathways in California, Environ Sci Technol, 53, 7163-7171, 10.1021/acs.est.9b02385, 2019a.

Zhao, B., Wang, S., Ding, D., Wu, W., Chang, X., Wang, J., Xing, J., Jang, C., Fu, J. S., and Zhu, Y.: Nonlinear relationships between air pollutant emissions and PM2. 5-related health impacts in the Beijing-Tianjin-Hebei region, Science of The Total Environment, 661, 375-385, 2019b.

Zhao, Y., Zhang, K., Xu, X., Shen, H., Zhu, X., Zhang, Y., Hu, Y., and Shen, G.: Substantial Changes in Nitrate Oxide and Ozone after Excluding Meteorological Impacts during the COVID-19 Outbreak in Mainland China, Environmental Science & Technology Letters, 7, 402-408, 2020.
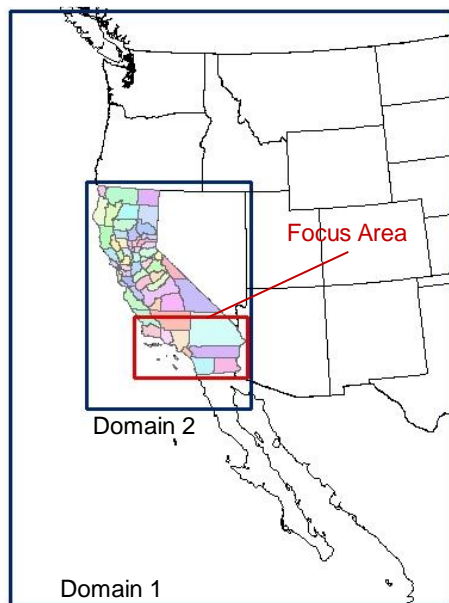
540 **Figure 1: Simulation domains of this study. The red rectangle denotes the area of southern California where most analyses in this study focus on.**
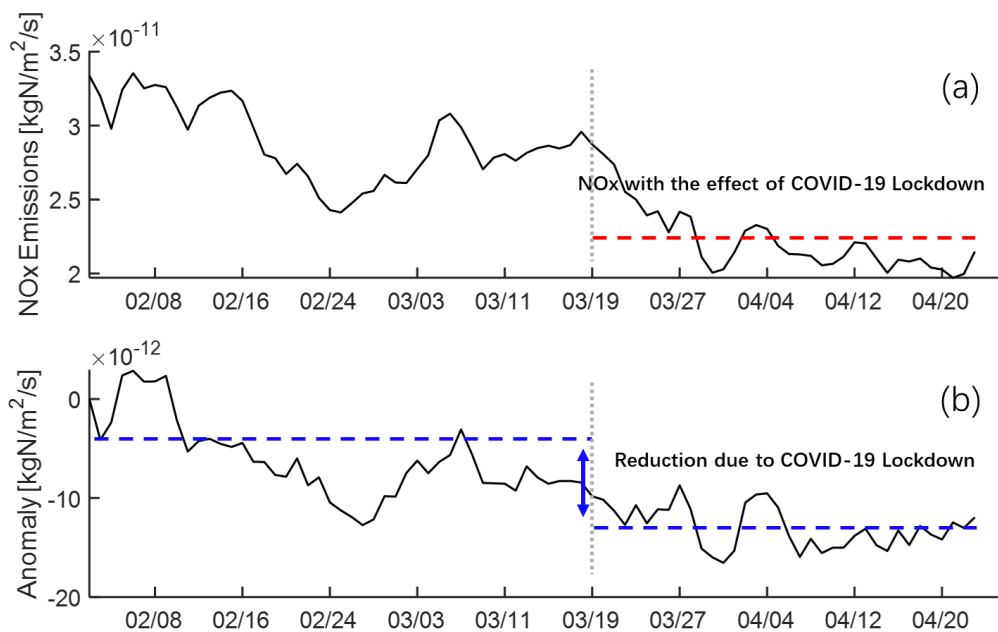
Figure 2: Satellite-derived NO$_x$ emission estimates in southern California. (a) Daily NO$_x$ emissions from February 1 to April 23, 2020. The red line represents the average emissions during the period after March 19. (b) NO$_x$ emission changes due to the
545 **COVID-19 (i.e., the anomaly), which is quantified using the difference between the real-world NO$_x$ emissions and the emissions in**

a hypothetical scenario without considering the COVID-19. The emissions in the hypothetical scenario is estimated based on emission trends in prior years (2017–2019), using February 1 as a reference. The difference between two blue dashed lines represents the average reductions of NO_x emissions induced by the COVID-19 lockdown measures that took effect on March 19. The local valley between February 24 and March 3 is caused by retrieval uncertainties caused by unfavorable meteorology

550   conditions and is thus excluded when we estimate the average NO_x emissions before the lockdown.
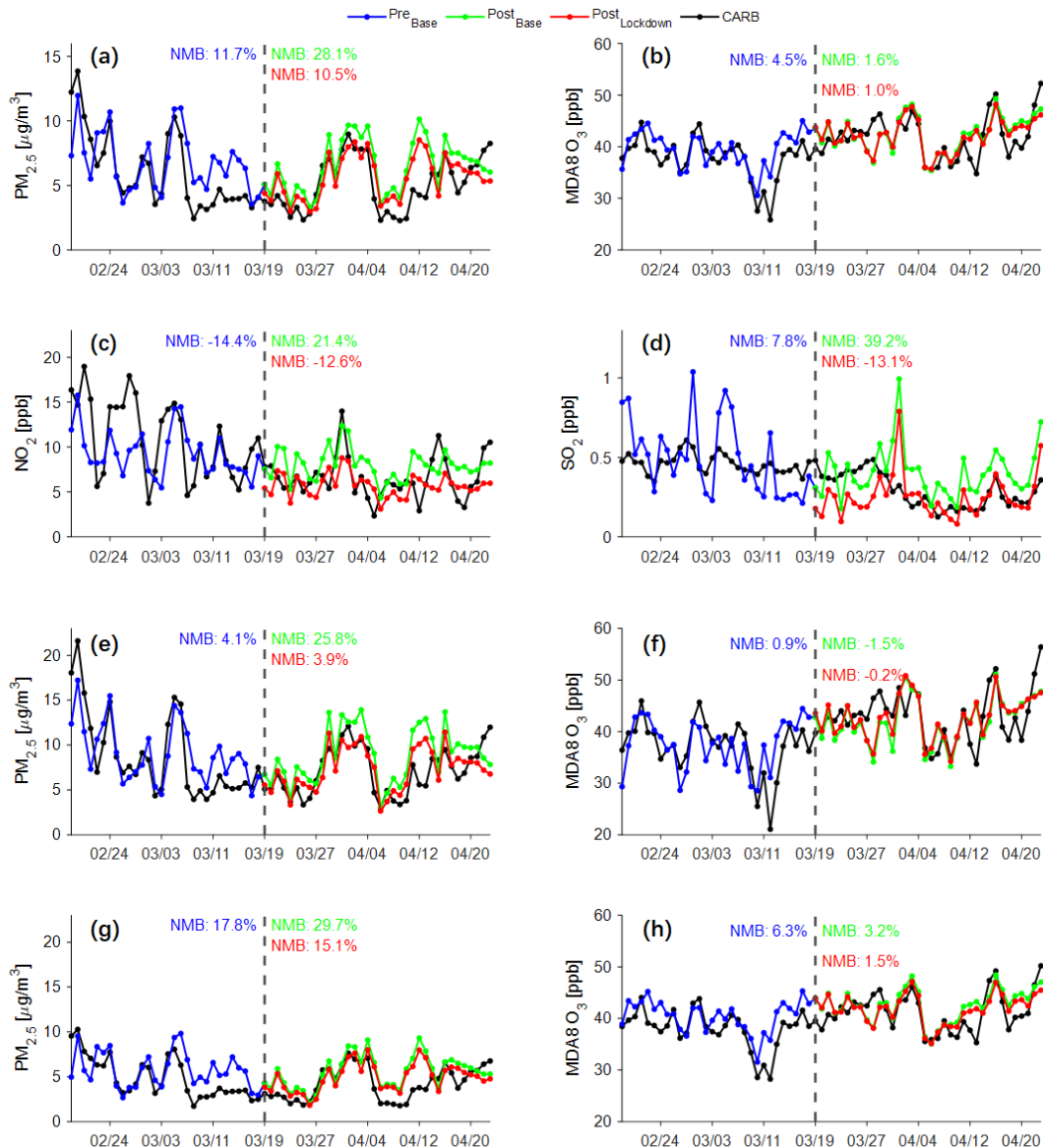
Figure 3: Time series of observed and simulated concentrations of major pollutants. (a-d) Time series of (a) PM2.5, (b) MDA8 O3, (c) NO2, and (d) SO2 averaged across all observational stations from CARB over southern California. (e-f) Time series of (e) PM2.5

555 and (f) MDA8 O₃ across all stations over the urban areas of southern California. (g-h) The same as (e-f) but for the rural areas. Black lines are surface observations from the CARB network. Blue, green, and red lines are simulated air pollutant concentrations during the pre-lockdown period (February 18 to March 18) under the Base scenario (Pre$_{Base}$), during the lockdown period (March 19 to April 23) under the Base scenario (Post$_{Base}$), and during the lockdown period under the Lockdown scenario (Post$_{Lockdown}$). The definitions of the Base and Lockdown scenarios are summarized in Table 1. Normalized mean bias (NMB) is given by $=$
560 $\sum_{i=1}^{N}(Var_m - Var_o)/\sum_{i=1}^{N}Var_o$, where N is the number of sites, Var$_m$ and Var$_o$ are modeled and observed concentrations, respectively.
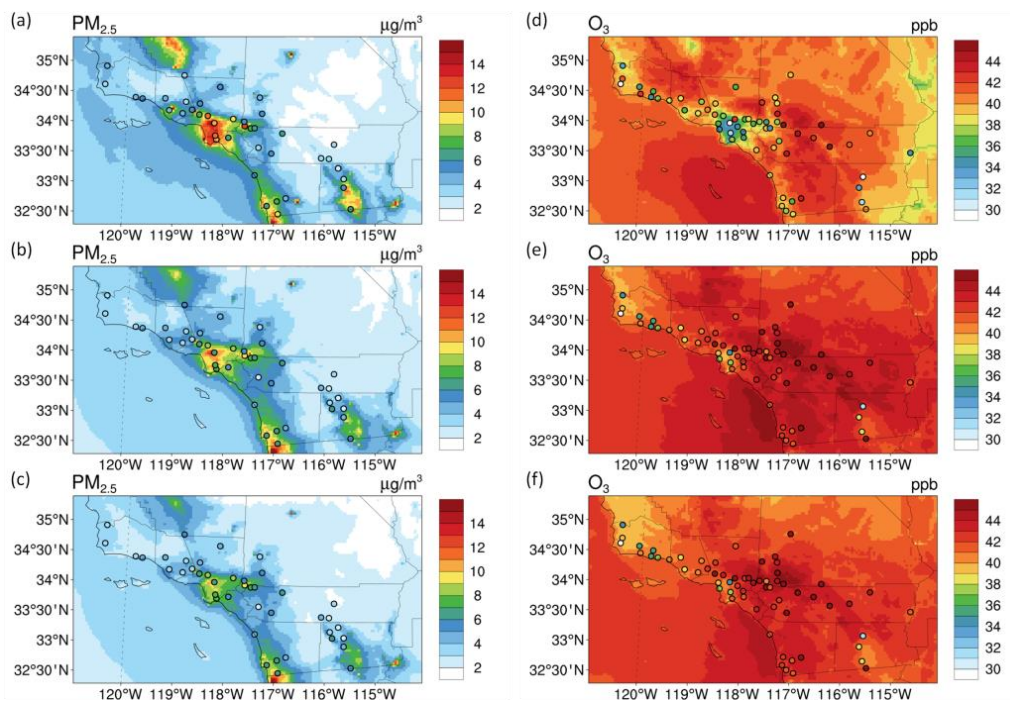
Figure 4: Overlay plots of the simulated (contour) and observed (circles) PM$_{2.5}$ and MDA8 O₃ concentrations in southern California. (a-c) are for PM$_{2.5}$ and (d-f) are for MDA8 O₃. (a, d) are for the pre-lockdown period (February 18 to March 18) under
565 the Base scenario (Pre$_{Base}$); (b, e) are for the lockdown period (March 19 to April 23) under the Base scenario (Post$_{Base}$); (c, f) are for the lockdown period under the Lockdown scenario (Post$_{Lockdown}$).
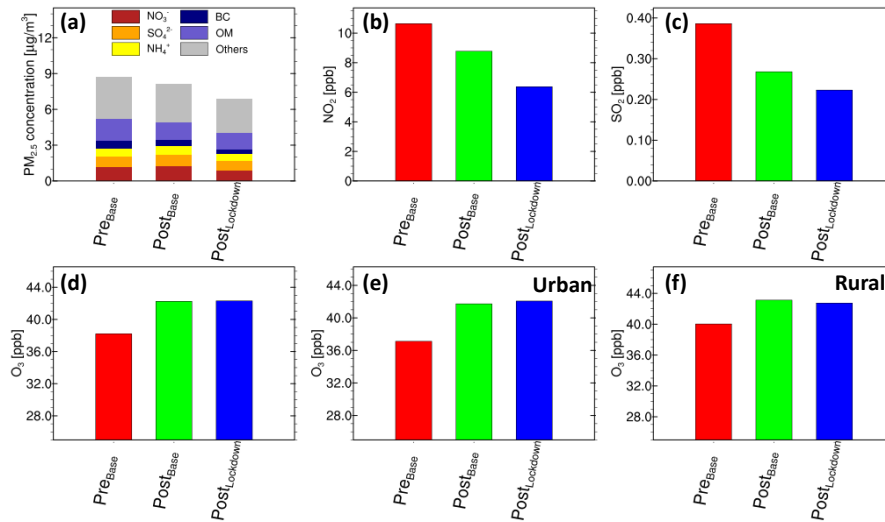
Figure 5: Effects of emission reductions and meteorology conditions on air pollutants. (a-d) Population-weighted concentrations of simulated air pollutant concentrations in southern California: (a) PM$_{2.5}$ components; (b) NO$_2$; (c) SO$_2$; (d) MDA8 O$_3$ over southern California; (e) MDA8 O$_3$ over the urban areas of southern California; (f) MDA8 O$_3$ over the rural areas of southern California. Pre$_{Base}$, Post$_{Base}$, and Post$_{Lockdown}$ have the same meanings as in Fig. 3.
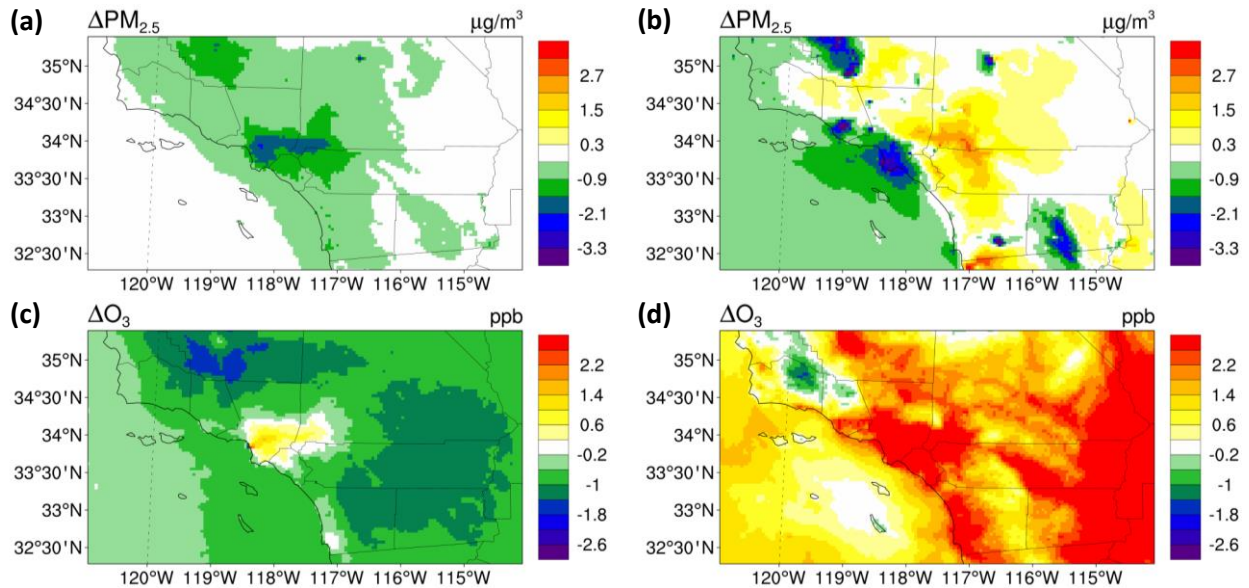
Figure 6: Spatial distributions of the emission reductions and meteorology conditions effects on air pollutants. (a, c) emission reductions and (b, d) meteorology variations on (a,b) PM$_{2.5}$ and (c, d) MDA8 O$_3$ concentrations.

=
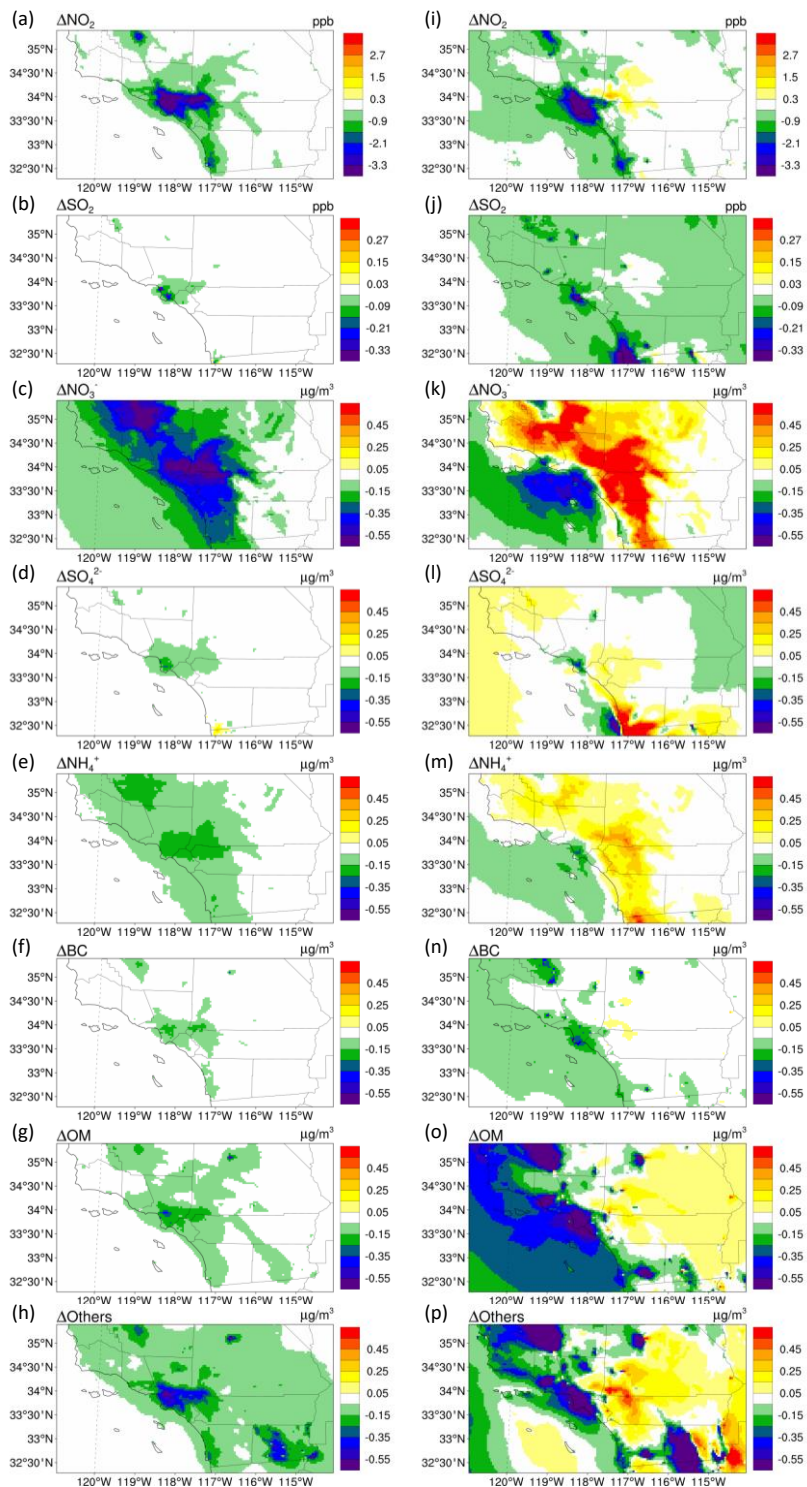
Figure 7: The same as Figs. 6 but for NO₂, SO₂, and different PM2.5 chemical components.

580
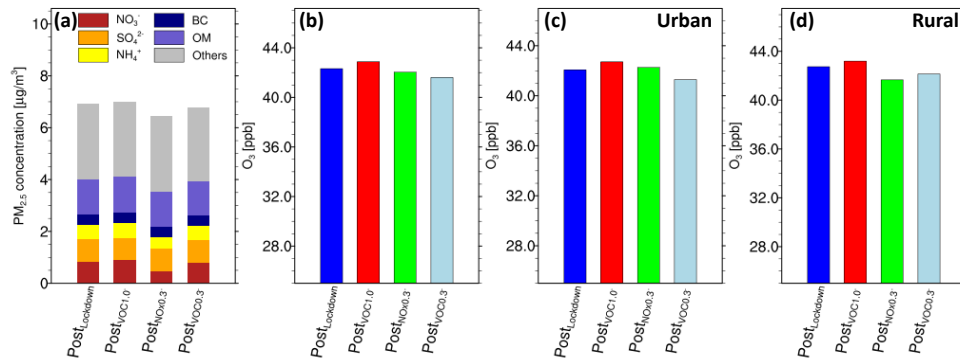
Figure 8: Simulated population-weighted PM2.5 and O3 concentrations under three sensitivity scenarios (VOC1.0, NOx0.3 and VOC0.3) during the lockdown period (March 19 to April 23) over southern California. (a) PM2.5 components, (b) MDA8 O3, (c) MDA8 O3 over the urban areas, and (d) MDA8 O3 over the rural areas. The definitions of all scenarios are summarized in Table 1.
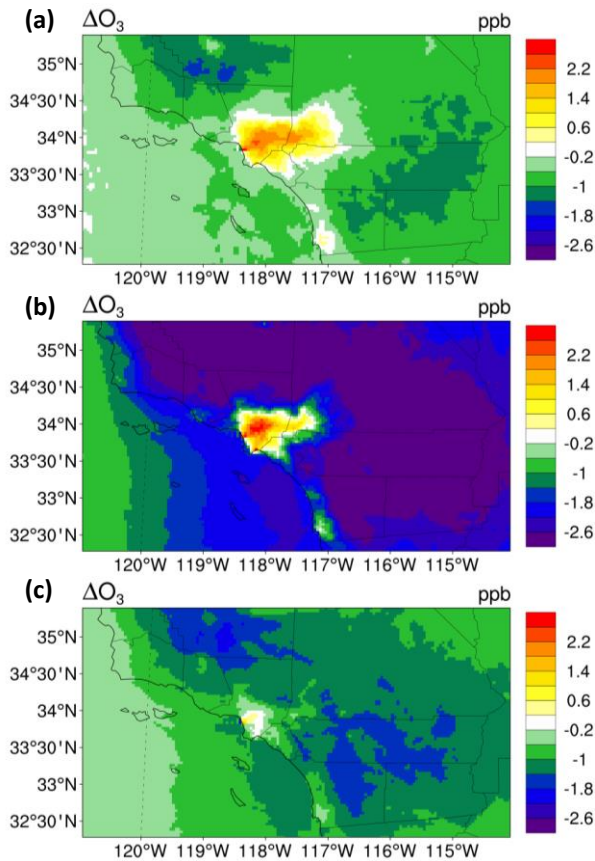
585 **Figure 9: Spatial distribution of the differences in MDA8 O₃ between the three sensitivity scenarios and the Base scenario: (a) VOC1.0 minus Base; (b) NOₓ0.3 minus Base; (c) VOC0.3 minus Base. The definitions of all scenarios are summarized in Table 1.**
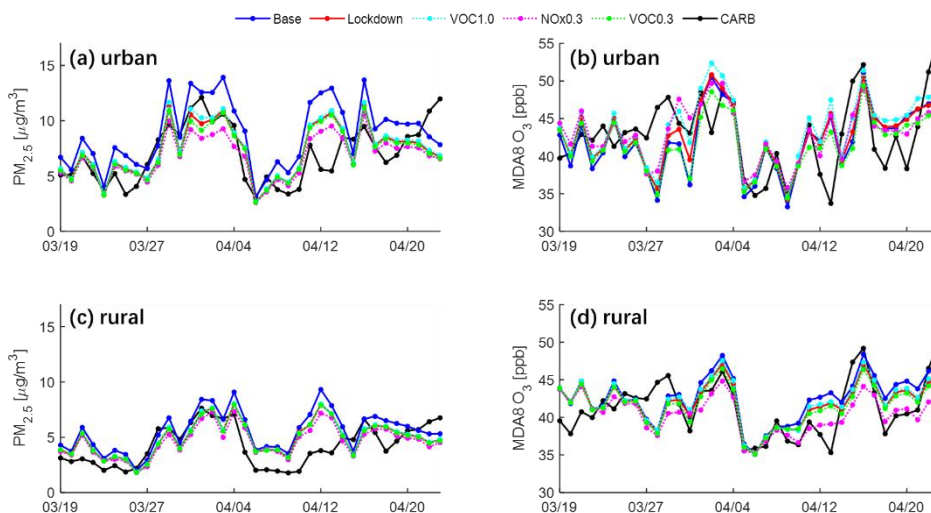
Figure 10: Time series of simulated and observed PM$_{2.5}$ concentrations (a, c) and MDA8 O$_3$ concentrations (b, d) under several sensitivity scenarios averaged across the CARB observational stations over the urban (a, b) and rural (c, d) areas of southern
590 **California during the lockdown period (March 19 to April 23). Black lines are surface observations from CARB networks. Blue, red, cyan, magenta, and green lines are simulated results for the Base, Lockdown, VOC1.0, NO$_x$0.3, and VOC0.3 scenarios. The definitions of all scenarios are summarized in Table 1.**

Table 1. Summary of model scenarios developed in this study.

Scenario	Definition
Base	This scenario uses the default CARB emission inventory without considering the emission reductions induced by the COVID-19 lockdown. It provides a baseline for evaluating the effect of COVID-19 lockdown on air quality.
Lockdown	This scenario adjusts the CARB emission inventory to account for the emission reductions due to the COVID-19 lockdown. The difference between "Base" and "Lockdown" represents the effect of the COVID-19 lockdown.
VOC1.0	This scenario is the same as "Lockdown" except that the VOC emissions are kept at the level of the "Base" scenario. It is used to evaluate the relative contribution of VOC and NO$_x$ reductions to COVID-19 induced O$_3$ concentration changes.
NO$_x$0.3	This scenario is the same as "Lockdown" except that the NO$_x$ emissions are further reduced to 30% of those in the "Base" scenario. It is used to assess the potential effects of strengthened NO$_x$ control measures.
VOC0.3	This scenario is the same as "Lockdown" except that the VOC emissions are further reduced to 30% of those in the "Base" scenario. It is used to assess the potential effects of strengthened VOC control measures.

595

22

Table 2. The percentage of changes in air pollutant emissions during the COVID-19 lockdown relative to a hypothetical scenario without the lockdown in southern California.

	VOC	CO	NO$_X$	SO$_X$	PM$_{10}$	PM$_{2.5}$	NH$_3$
Onroad transportation	-50%	-51%	-39%	-35%	-44%	-42%	-51%
Off-road transportation	-30%	-30%	-30%	-30%	-30%	-30%	-30%
Aircraft	-70%	-70%	-70%	-70%	-70%	-70%	-70%
Power plants	-7%	-7%	-7%	-7%	-7%	-7%	-7%
Industrial	-15%	-15%	-15%	-15%	-15%	-15%	-15%
Residential	10%	10%	10%	10%	10%	10%	10%
Commercial	-15%	-15%	-15%	-15%	-15%	-15%	-15%
Agriculture	0%	0%	0%	0%	0%	0%	0%
Total	-21.1%	-35.7%	-28.3%	-18.5%	-9.7%	-15.0%	-16.1%

Table 3. Evaluation of meteorological simulation results as compared to observational data from the National Climatic Data Center.

Variable	Index	Value	Ref[a]	Variable	Index	Value	Ref[a]
Wind speed (m/s)	Mean observation	3.92		Temperature (K)	Mean observation	287.48	
	Mean simulation	3.69			Mean simulation	287.21	
	Mean Bias	-0.22	≤ ±0.5		Mean Bias	-0.28	≤ ±0.5
	Gross error	1.43	≤2		Gross error	1.76	≤2
	IOA[b]	0.76	≥0.6		IOA	0.93	≥0.8
Wind direction (deg)	Mean observation	243.45		Humidity (g/kg)	Mean observation	6.41	
	Mean simulation	232.90			Mean simulation	6.16	
	Mean Bias	1.48	≤ ±10		Mean Bias	-0.25	≤ ±1
	Gross error	44.53	≤30		Gross error	0.83	≤2
					IOA	0.84	≥0.6